Scripta Materialia 213 (2022) 114641

Contents lists available at ScienceDirect

Scripta Materialia

journal homepage: www.journals.elsevier.com/scripta-materialia

Helium-induced swelling and mechanical property degradation in ultrafine-grained W and W-Cu nanocomposites for fusion applications

Michael Wurmshuber [a,*], Mehdi Balooch [b], Xi Huang [b], Peter Hosemann [b,c], Daniel Kiener [a]

[a] Department Materials Science, Chair of Materials Physics, Montanuniversität Leoben, Jahnstraße 12, Leoben 8700, Austria
[b] Department of Nuclear Engineering, University of California, Berkeley, 4155 Etcheverry Hall, Berkeley, CA 94720, USA
[c] Materials Sciences Division, Lawrence Berkeley National Laboratory, 1 Cyclotron Road, Berkeley, CA 94720, USA

A B S T R A C T

Besides high dose radiation and extreme thermal loads, a major concern for materials deployed in novel nuclear fusion reactors is the formation and growth of helium bubbles. This work investigates the swelling and mechanical property degradation after helium implantation of ultrafine-grained W and nanocrystalline W-Cu, possible candidates for divertor and heat-sink materials in fusion reactors, respectively. It is found that ultrafine-grained W and single crystalline W experience similar volumetric swelling after helium implantation but show different blistering behavior. The W-Cu nanocomposite, however, shows a reduced swelling compared to a coarse-grained composite due to the effective annihilation of radiation-induced vacancies through interfaces. Furthermore, the helium-filled cavity structures lead to considerable softening of the composite.

The effects of helium as a transmutation product in structural nuclear reactor materials have been investigated since the early days of nuclear engineering [1,2]. In-service fission devices, such as currently operating CANDU reactors [3,4], serve as reminders that helium gas in structural materials can lead to materials challenges. Furthermore, the renewed interest in nuclear fusion and the recent efforts in commercializing fusion technology led to an increase in associated research. In addition to radiation effects on materials in fusion environments and transmutation reactions, the fusion reaction itself ${}^{2}_{1}D + {}^{3}_{1}T \rightarrow {}^{4}_{2}He + n +$ 17.6 *MeV* generates helium ions that can interact with the plasma-facing wall material [5]. Therefore, in addition to well researched radiation effects [1,2,6,7] and extreme thermals loads, one has to account for helium bubble nucleation and growth within the structural materials employed in the vicinity or even facing the fusion plasma. For the divertor, the part of the reactor experiencing the prevalent exposure to the plasma, tungsten is often considered the prime candidate material due to a plethora of advantageous physical properties [8,9]. In particular, ultrafine-grained (ufg) W is an exciting prospect, as the small grain size has beneficial effects on mechanical properties, such as fracture toughness [10,11]. Moreover, to allow for a rapid heat transport away from the divertor and avoid temperature fluctuation-induced failure of the component, high strength heat sinks have to be employed, commonly in the form of W-Cu composite materials [12,13]. Here a nanostructuring of the composite is beneficial for radiation tolerance and mechanical strength [6].

While helium implantation of single-crystalline (sxx) and coarse-grained (cg) W and Cu have been investigated thoroughly in earlier works [14–17], for ufg W most work focuses on bubble evolution and morphology [18–20]. These insights provide a fundamental understanding of the microstructural changes arising from helium implantation, but the concrete implications for swelling and changes in mechanical properties (i.e. elastic modulus and hardness) of the implanted material will define the practical employment of ufg W and W-Cu composites in fusion reactors. In this work, a combined approach of atomic force microscopy (AFM) and nanoindentation was utilized to investigate the swelling and related changes in mechanical properties of ufg W and nanocrystalline (nc) W-Cu as implanted with various fluences of helium.

Ufg W and nc W-Cu composites are fabricated from powders using severe plastic deformation. W powder (purity 99.97%, particle size <2 μm, Plansee SE, Austria) is stored, handled and compacted within argon atmosphere. An intermediate annealing step after compacting at 1600 °C for 7 h in a vacuum-furnace (Leybold Heraeus PD 1000, Leybold GmbH, Germany) assures sufficient particle bonding before severe plastic deformation is applied through a high-pressure torsion (HPT) tool [21] for 1 rotation at a nominal pressure of 12 GPa and a temperature of 400 °C. More details regarding the fabrication of ufg W can be found in references [11,22]. The grain size of ufg W was measured from micrographs (Fig. 1a) using the line intercept method and is 158 ± 35 nm (125 ± 10 nm in implantation direction and 189 ± 21 nm in lateral

* Corresponding author.
E-mail address: michael.wurmshuber@unileoben.ac.at (M. Wurmshuber).

https://doi.org/10.1016/j.scriptamat.2022.114641
Received 17 January 2022; Received in revised form 23 February 2022; Accepted 24 February 2022
Available online 2 March 2022

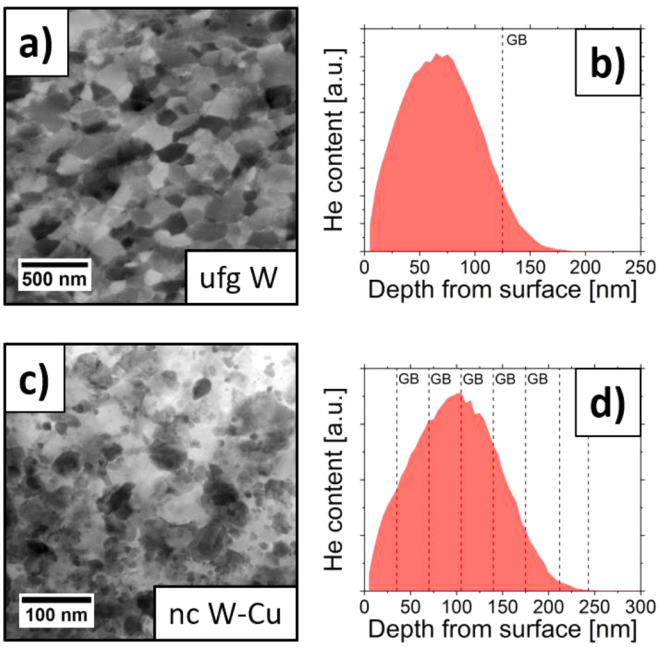

Fig. 1. Microstructures of (a) ufg W (SEM) and (c) nc W-Cu (TEM). The penetration depths of 25 keV He ions for (b) ufg W and (d) nc W-Cu were simulated by SRIM. Vertical lines indicate the average location of grain boundaries.

direction). For the W-Cu nanocomposite, 25 at.% of the respective W powder and 75 at.% Cu powder (purity 99%, particle size 14–25 μm, Merck KGaA, Germany) were mixed within argon atmosphere and then compacted using the HPT tool. The powder compact was subsequently deformed using the HPT for 100 revolutions under a pressure of 9 GPa at room temperature. The grains were measured from TEM images (Fig. 1c) to be 35 ± 17 nm in diameter and equiaxed.

A helium-ion microscope (Orion Nanofab, Carl Zeiss GmbH, Germany) [16,23,24] was used to implant 25 keV helium ions to fluences of 6×10^{17} and 10^{18} ions/cm^2 in ufg W and 3×10^{17}, 6×10^{17} and 10^{18} ions/cm^2 in nc W-Cu. The helium was implanted on 10×10 μm^2 squares on the polished surfaces with a dose rate of about 1 dpa/min. The implantations of both materials have been simulated using the software "Stopping Range of Ions in Matter" (SRIM) [25] using the Kinchin-Pease model and displacement energies of 85 eV for W [26,27] and 30 eV for Cu [26,28]. The calculated helium ion profiles are depicted in Fig. 1b,d. For the W-Cu composite, a hypothetical solid solution was chosen as model material for the simulations. This represents a satisfying average of the irradiation response, even though W is expected to exert a higher stopping effect than Cu. This behavior leads to local deviations from the averaged profile in Fig. 1d, depending on the distribution of W and Cu grains inside the material hit by the He beam, but will not influence the average penetration depth significantly.

Subsequent to implantation, the surface topology of and around the implanted areas on both materials was scanned using an atomic force microscope (AFM; Nanoscope III, Digital Instruments, USA) in tapping mode. This way, the amount of surface swelling due to helium bubble formation can be measured by comparing the average height difference of the implanted regions to the unimplanted surface, a quantity commonly referred to as swelling height [14,16,24] (see Fig. 2a). Fig. 2b displays the compiled results of the swelling measurements of ufg W and nc W-Cu, as well as extrapolated values for swelling of sxx W [14] and cg ("quasi-sxx") Cu [16]. Additionally, a simple arithmetic combination of cg Cu and sxx W values in the same ratio as the investigated composite (25 at.% W + 75 at.% Cu) is shown. Naturally, for all materials the swelling increases with increasing helium fluence. No swelling data could be acquired for the fluence of 3×10^{17} ions/cm^2 in ufg W, as this implantation unfortunately failed.

From Fig. 2b it is apparent that Cu and the W-Cu composite exhibit a higher swelling than the pure W samples. This is rationalized by the fact that Cu has an fcc crystal structure, which is more densely packed and known to be more sensitive to void and gas bubble swelling than bcc metals [29,30]. The nc W-Cu investigated in this work displays far less swelling than the arithmetic combination of cg Cu and sxx W values. This proves that the vast amount of grain boundaries and interfaces within the nc W-Cu has a significant influence on bubble formation and growth and, therefore, the resulting swelling. Swelling of the ufg W material, however, is comparable to the sxx W investigated by Allen et al. [14]. It appears that the still large amount of grain boundaries within the ufg W does not have any noticeable effect on the measured swelling height, which is supported by the findings of El-Atwani et al. [20], reporting a grain size threshold of 35–50 nm in W. Above this threshold helium bubble size and density, and thus swelling, are not

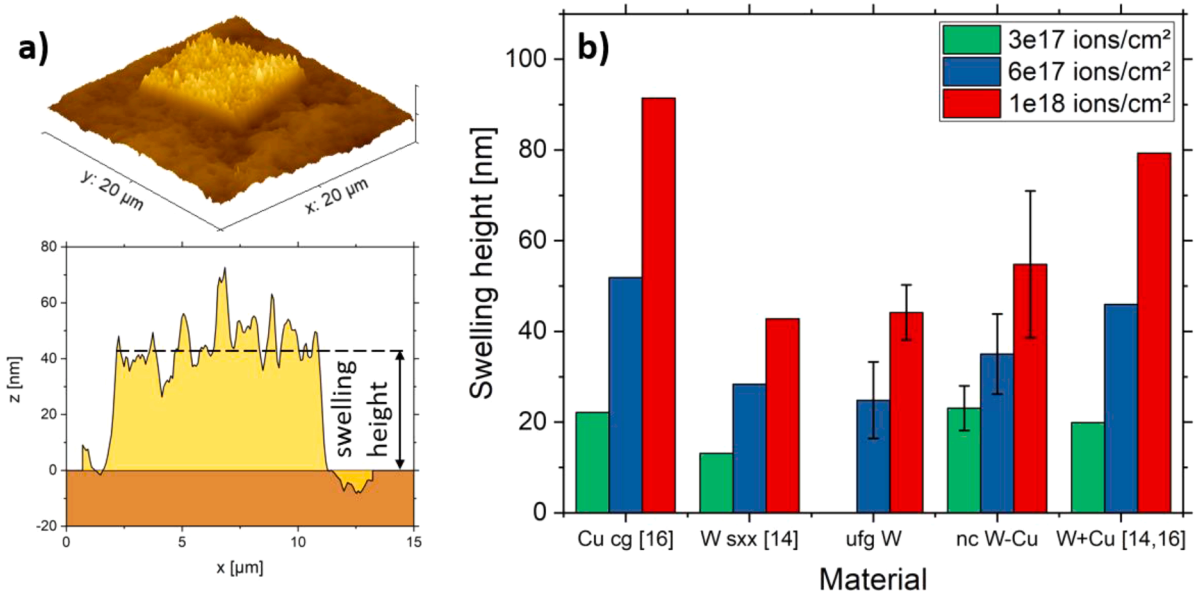

Fig. 2. (a) Representative AFM image of ufg W implanted with a helium fluence of 10^{18} ions/cm^2 and schematic on the definition of swelling height. (b) Swelling height of ufg W and nc W-Cu compared to literature data for cg Cu and sxx W. Error bars represent the RMS roughness on the implanted squares.

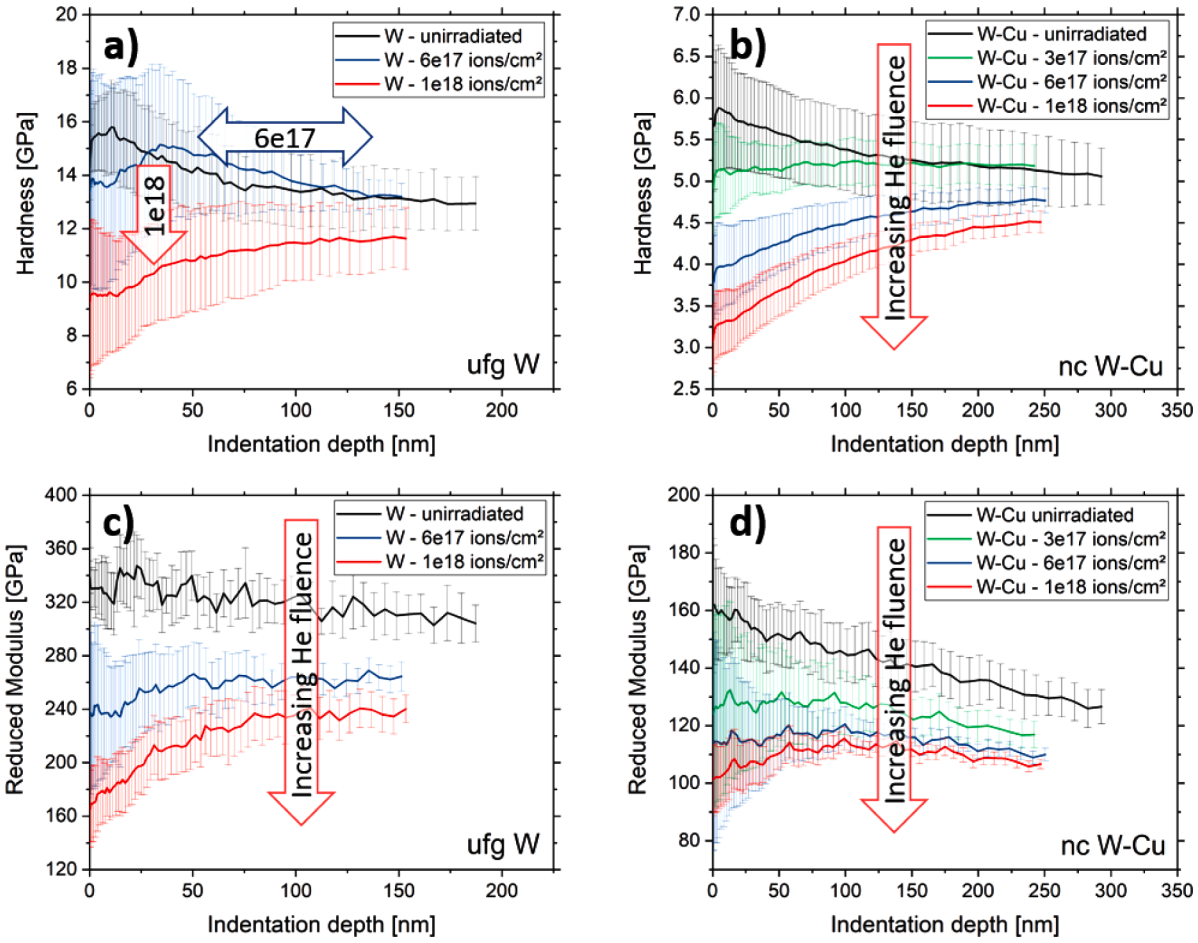

Fig. 3. Averaged nanoindentation curves for hardness (a,b) and reduced modulus (c,d) of ufg W (a,c) and nc W-Cu (b,d). Both moduli and the hardness of nc W-Cu decrease with increasing He fluence. The hardness of ufg W stays preserved after implanting with a fluence of 6 x 10^{17} ions/cm^2 and decreases only at a higher fluence of 10^{18} ions/cm^2.

influenced significantly by the grain boundaries at room temperature, as the ability to effectively remove radiation-induced vacancies is not given. Furthermore, as visualized in Fig. 1b, on average only a single grain boundary, located far beyond the peak of helium content, lies within the helium implanted region in implantation direction. In comparison, in the W-Cu nanocomposite the smaller grain size and larger penetration depth result in up to seven grain boundaries being located in the helium-affected zone on average (Fig. 1d). There are of course more grain boundaries in the lateral direction of the implanted area, which could lead to a more pronounced swelling in the horizontal direction. When assuming simple brick-shaped grains, the grain boundary area within the affected zone accumulates to roughly 340 μm^2 in ufg W and 1410 μm^2 in nc W-Cu. This significant difference provides an additional explanation as to why the grain size of ~35 nm is so much more effective in reducing swelling than a grain size of ~150 nm. It should be noted, however, that blisters as observed for sxx W in [14] are not present in the ufg W sample implanted with similar helium fluences (see Fig. 2a), indicating that bubble growth and coalescence are restricted, and bubble nucleation is the main reason for the comparable swelling heights of the two materials. All things considered, the nc W-Cu shows still a higher swelling than either W material, which confirms that W, and bcc materials in general, demonstrate a high resistance to helium bubble swelling. While this resistance could potentially be amplified by reducing the grain size further, following the idea of [20], this would in turn deteriorate the excellent ductility and fracture toughness that ufg W showcases [10,11].

Turning from swelling to related changes in mechanical properties, the small penetration depth of the helium ions in W and W-Cu makes it challenging to assess irradiation-induced changes. A number of various small-scale testing methods have been applied in the past to assess irradiation induced property changes of ion-irradiated materials [16,24,31–33]. Nanoindentation offers several advantages, such as absence of additional sample preparation as well as easy and straightforward testing. By applying dynamic continuous stiffness measurements (CSM) [34–37], hardness and modulus can be probed along the indentation depth. In this work, a TI 950 Triboindenter (Hysitron Inc., USA) with a CSM and a Scanning Probe Microscopy (SPM) option was used to indent the implanted and unimplanted areas. After the Berkovich tip was calibrated on fused silica following Oliver & Pharr [34], the implanted area was scanned using the SPM option. Indents were placed inside and outside of the implanted squares to an indentation depth of about 200 nm in the ufg W material and 300 nm in the W-Cu nanocomposite. For every material condition, 4-5 nanoindentation tests were conducted. Considering the small penetration depth of the helium ions of about 180 nm (W) to 230 nm (W-Cu) (Fig. 1b,d), the indentation tests will always probe additional unaffected material below the implanted helium layer, thus not reflecting only the hardness of the implanted layer. However, the trend of hardening and softening through helium implantation

should still be apparent in the results, albeit less pronounced for larger indentation depths [31,32].

The averaged nanoindentation curves plus standard deviation for every condition are presented in Fig. 3. It is obvious that the reduced elastic modulus of both ufg W and nc W-Cu decreases continuously with increasing helium fluence (Fig. 3c,d). This is explained by the continued formation and growth of helium bubbles within the materials with more helium being implanted. Regarding hardness, the two materials show a slightly different behavior. While the hardness of the nanocomposite decreases continuously with increasing fluence (see Fig. 3b), the ufg W seems to retain its hardness after implantation with a fluence of 6×10^{17} ions/cm^2 and only deteriorate after implantation with a higher fluence of 10^{18} ions/cm^2 (see Fig. 3a). This is most likely deceiving, as earlier work by the authors unveiled for Cu-Fe-Ag with similar grain size that for such ufg materials, a combination of conventional radiation hardening (dominant at lower fluences) and softening through gas bubble nucleation and growth (dominant at higher fluences) is the reason for a perceived sustained hardness from the unirradiated state at fluences around 4–6 $\times$ 10^{17} ions/cm^2 [24]. It is crucial to note that, while the hardness is seemingly unchanged, a critical reduction in ductility and toughness can be expected from these competing hardening and softening mechanisms. For the nc W-Cu composite this effect is not observed, as the much smaller grain size of about 35 nm leads to the efficient annihilation of radiation-induced point defects, thereby suppressing the radiation hardening effect [6,7]. Without such a hardening effect, the size and amount of helium gas bubbles are the major factors influencing the mechanical properties, leading to softening throughout all fluences of helium implantation [24]. Commonly, in single-crystalline metals or metals with grain sizes above 1 μm, such a softening effect is not observed, especially for low fluences. Here, the formed helium bubbles act as obstacles to dislocation movement within the grains and lead to a pronounced hardening effect [38–40]. In contrast, in nc and ufg metals bubbles nucleate preferably at GBs, where they do not interfere with dislocation propagation. The softening effect can therefore be explained by the slow transformation of the material into a metal foam and a facilitated dislocation nucleation from bubble-decorated GBs, in agreement with other works [7,24,41,42].

In summary, swelling and mechanical property changes of ufg W and nc W-Cu were assessed after implantation with helium ions. While the W-Cu nanocomposite experiences more swelling than the ufg W due to the contained fcc Cu phase, a reduction of swelling compared to cg Cu and a cg W-Cu composite could be achieved via the small grain size of 35 nm. In contrast, aside from the lack of blister formation, the grain size of 158 nm in ufg W led to no significant changes in measured swelling compared to sxx W. This is explained by the much lower grain boundary area density of ufg W and by the inability to remove vacancies before they nucleate bubbles at a grain size above 50 nm. Similarly, this inability results in a combined radiation-induced hardening and bubble-induced softening effect when probing the mechanical properties of helium-implanted W. As the hardening effect is absent in nc W-Cu, the hardness deteriorates much faster due to the suppressed but still present bubble formation and growth. In conclusion, while the ufg grain size improves the overall mechanical properties of W, the implications for swelling resistance are minor. The nc grain size of W-Cu, however, results in significantly reduced bubble-induced swelling, but also quick degradation of hardness and modulus due to the absence of radiation hardening. The findings presented in this work are expected to contribute to an improved understanding on how promising ultrafine- and nano-grained materials perform in the harsh environment of a nuclear fusion reactor.

Declaration of Competing Interest

The authors declare that they have no known competing financial interests or personal relationships that could have appeared to influence the work reported in this paper.

Acknowledgments

The authors acknowledge funding by the European Research Council under Grant No. 771146 (TOUGHIT). Additional financial support was provided by the Austrian Marshall Plan Foundation. The authors acknowledge further support from NSF DMR Award No. 1807822. The authors thank Dr. Michael Burtscher for providing TEM images of the W-Cu nanocomposite and Simon Doppermann for help with sample fabrication.

References

[1] D.R. Olander, Fundamental Aspects of Nuclear Reactor Fuel Elements, Technical Information Center, Office of Public Affairs, Energy Research and Development Administration, Springfield, USA, 1977.
[2] G.S. Was, Fundamentals of Radiation Materials Science, Springer Berlin Heidelberg, New York, 2007.
[3] M. Griffiths, AECL Nucl. Rev. 2 (2013) 1–16.
[4] C. Howard, V. Bhakhri, C. Dixon, H. Rajakumar, C. Mayhew, C.D. Judge, J. Nucl. Mater. 517 (2019) 17–34.
[5] E. Rebhan, D. Reiter, R. Weynants, U. Samm, W.J. Hogan, J. Raeder, T. Hamacher, K. Heinloth, Landolt-Börnstein: Numerical Data and Functional Relationships in Science and Technology Gr. VIII Adv. Mater. Technol, Springer, 2005, pp. 304–368.
[6] X. Zhang, K. Hattar, Y. Chen, L. Shao, J. Li, C. Sun, K. Yu, N. Li, M.L. Taheri, H. Wang, J. Wang, M. Nastasi, Prog. Mater. Sci. 96 (2018) 217–321.
[7] M. Wurmshuber, D. Frazer, A. Bachmaier, Y. Wang, P. Hosemann, D. Kiener, Mater. Des. 160 (2018) 1148–1157.
[8] M. Rieth, D.E.J. Armstrong, B. Dafferner, S. Heger, A. Hoffmann, M. Hoffmann, U. Jäntsch, M. Rohde, T. Scherer, V. Widak, H. Zimmermann, Adv. Sci. Technol. 73 (2010) 11–21.
[9] M. Rieth, S.L. Dudarev, S.M.G. De Vicente, J. Aktaa, T. Ahlgren, S. Antusch, D.E. J. Armstrong, M. Balden, N. Baluc, M. Barthe, W.W. Basuki, M. Battabyal, C. S. Becquart, D. Blagoeva, H. Boldyryeva, J. Brinkmann, M. Celino, L. Ciupinski, J. B. Correia, A. De Backer, C. Domain, E. Gaganidze, C. Garcia-Rosales, J. Gibson, M. R. Gilbert, S. Giusepponi, B. Gludovatz, H. Greuner, K. Heinola, T. Höschen, A. Hoffmann, N. Holstein, F. Koch, W. Krauss, H. Li, S. Lindig, J. Linke, C. Linsmeier, P. López-Ruiz, H. Maier, J. Matejicek, T.P. Mishra, M. Walter, T. Weber, T. Weitkamp, S. Wurster, M.A. Yar, J.H. You, A. Zivelonghi, J. Nucl. Mater. 432 (2013) 482–500.
[10] M. Faleschini, H. Kreuzer, D. Kiener, R. Pippan, J. Nucl. Mater. 367–370 (2007) 800–805.
[11] M. Wurmshuber, S. Jakob, S. Doppermann, S. Wurster, R. Bodlos, L. Romaner, V. Maier-Kiener, D. Kiener, Submitt. to Acta Mater. (n.d.).
[12] O.A. Waseem, H.J. Ryu, R. Rahman, Nuclear Materials Performance, IntechOpen, 2016, pp. 139–161.
[13] E. Tejado, Mater. Today 38 (2020) 136–137.
[14] F.I. Allen, P. Hosemann, M. Balooch, Scr. Mater. 178 (2020) 256–260.
[15] Z. Chen, L.L. Niu, Z. Wang, L. Tian, L. Kecskes, K. Zhu, Q. Wei, Acta Mater. 147 (2018) 100–112.
[16] Y. Yang, D. Frazer, M. Balooch, P. Hosemann, J. Nucl. Mater. 512 (2018) 137–143.
[17] W. Han, E.G. Fu, M.J. Demkowicz, Y. Wang, A. Misra, J. Mater. Res. 28 (2013) 2763–2770.
[18] O. El-Atwani, J.A. Hinks, G. Greaves, S. Gonderman, T. Qiu, M. Efe, J.P. Allain, Sci. Rep. 4 (2014) 4–10.
[19] O. El-Atwani, K. Hattar, J.A. Hinks, G. Greaves, S.S. Harilal, A. Hassanein, J. Nucl. Mater. 458 (2015) 216–223.
[20] O. El-Atwani, J.A. Hinks, G. Greaves, J.P. Allain, S.A. Maloy, Mater. Res. Lett. 5 (2017) 343–349.
[21] R. Pippan, S. Scheriau, A. Hohenwarter, M. Hafok, Mater. Sci. Forum 584–586 (2008) 16–21.
[22] M. Wurmshuber, S. Doppermann, S. Wurster, D. Kiener, IOP Conf. Ser. Mater. Sci. Eng. 580 (2019), 012051.
[23] F.I. Allen, Beilstein J. Nanotechnol. 12 (2021) 633–664.
[24] M. Wurmshuber, D. Frazer, M. Balooch, I. Issa, A. Bachmaier, P. Hosemann, D. Kiener, Mater. Charact. 171 (2021), 110822.
[25] J.F. Ziegler, J.P. Biersack, "SRIM - The Stopping and Range of Ions in Solids", 1985.
[26] A.Y. Konobeyev, U. Fischer, Y.A. Korovin, S.P. Simakov, Nucl. Energy Technol. 3 (2017) 169–175.

[27] M.J. Banisalman, S. Park, T. Oda, J. Nucl. Mater. 495 (2017) 277–284.
[28] E.A. Kenik, T.E. Mitchell, Philos. Mag. 32 (1975) 815–831.
[29] F.A. Garner, M.B. Toloczko, B.H. Sencer, J. Nucl. Mater. 276 (2000) 123–142.
[30] A. Bhattacharya, S.J. Zinkle, Cavity Swelling in Irradiated Materials. Comprehensive Nuclear Materials, Elsevier, 2020.
[31] D. Kiener, A.M. Minor, O. Anderoglu, Y. Wang, S.A. Maloy, P. Hosemann, J. Mater. Res. 27 (2012) 2724–2736.
[32] P. Hosemann, C. Shin, D. Kiener, J. Mater. Res. 30 (2015) 1231–1245.
[33] P. Hosemann, Scr. Mater. 143 (2018) 161–168.
[34] W.C. Oliver, G.M. Pharr, J. Mater. Res. 7 (1992) 1564–1583.
[35] W.C. Oliver, G.M. Pharr, J. Mater. Res. 19 (2004) 3–20.
[36] G.M. Pharr, J.H. Strader, W.C. Oliver, J. Mater. Res. 24 (2009) 653–666.
[37] A. Leitner, V. Maier-Kiener, D. Kiener, Mater. Res. Lett. 5 (2017) 486–493.
[38] F. Kong, M. Qu, S. Yan, A. Zhang, S. Peng, J. Xue, Y. Wang, Nucl. Instrum. Methods Phys. Res. Sect. B Beam Interact. Mater. Atoms 406 (2017) 643–647.
[39] J.T. Li, I.J. Beyerlein, W.Z. Han, Acta Mater. 226 (2022), 117656.
[40] W. Qin, Y. Wang, M. Tang, F. Ren, Q. Fu, G. Cai, L. Dong, L. Hu, G. Wei, C. Jiang, J. Nucl. Mater. 502 (2018) 132.
[41] W.S. Cunningham, J.M. Gentile, O. El-atwani, C.N. Taylor, M. Efe, S.A. Maloy, J. R. Trelewicz, Sci. Rep. 8 (2018) 1–10.
[42] H. Wang, F. Ren, J. Tang, W. Qin, L. Hu, L. Dong, B. Yang, G. Cai, C. Jiang, Acta Mater. 144 (2018) 691.